8 (2021) 100066

Contents lists available at ScienceDirect

Biosensors and Bioelectronics: X

journal homepage: www.journals.elsevier.com/biosensors-and-bioelectronics-x

Quantification and immunoprofiling of bladder cancer cell-derived extracellular vesicles with microfluidic chemiluminescent ELISA

Xiaotian Tan [a], Kathleen C. Day [b,c], Xuzhou Li [a,e], Luke J. Broses [b,c], Wen Xue [a], Weishu Wu [a], William Y. Wang [a], Ting-Wen Lo [d], Emma Purcell [d], Sicong Wang [e], Yun-Lu Sun [a], Maung Kyaw Khaing Oo [f], Brendon M. Baker [a], Sunitha Nagrath [c,d], Mark L. Day [b,c,**], Xudong Fan [a,*]

[a] Department of Biomedical Engineering, University of Michigan, Ann Arbor, MI, 48109, USA
[b] Department of Urology, University of Michigan, Ann Arbor, MI, 48109, USA
[c] Rogel Comprehensive Cancer Center, University of Michigan, Ann Arbor, MI, 48109, USA
[d] Department of Chemical Engineering, University of Michigan, Ann Arbor, MI, 48109, USA
[e] Department of Mechanical Engineering, University of Michigan, Ann Arbor, MI, 48109, USA
[f] Optofluidic Bioassay, LLC, Ann Arbor, MI, 48103, USA

A B S T R A C T

The functional membrane proteins on tumor-cell-derived EVs contain a large amount of biomolecular information, and can serve as a comprehensive marker to delineate the molecular nature of cancer. However, due to low secretion rates, it is difficult to perform accurate quantification and biomolecular analysis with conventional EV analysis technologies such as the Western blots. Here, we introduce a multifunctional EV analysis technology based on an automated microfluidic chemiluminescent ELISA (Enzyme-Linked ImmunoSorbent Assay) platform. With this system, we were able to achieve rapid EV quantification (<1 h) with relatively small sample volume (~8 μL) and high sensitivity (optimal LOD = 8.7×10^7 EV/mL). In addition to the EV quantification, we evaluated the expression levels for a panel of four cancer-related EV membrane proteins (EGFR, HER2, MHC-I, and EpCAM) using a newly developed immunoprofiling assay that combines immunoprecipitation and sandwich ELISA. Due to high sensitivity, this immunoprofiling assay only requires a very small amount of input protein (<40 ng/marker). Our studies show that the expression level of functional EV membrane proteins is stable under external stimulation, which suggests that the expression profile of the EV membrane proteins may serve as a robust and unique "molecular fingerprint" for the immunophenotyping of cancer cell lines.

Introduction

Extracellular vesicles (EVs) are the membrane-encapsulated vesicles secreted by eukaryotic cells. They can be broadly classified into exosomes, microvesicles (MVs), and apoptotic bodies according to their cellular origin (Gartz and Strande, 2018; Kalluri and LeBleu, 2020; Kowal et al., 2016). Out of them, nanometer-sized EVs (especially exosomes) are known to carrying multiple types of molecular information that reflect the phenotype of their "mother cells" (Azmi et al., 2013; Kalluri and LeBleu, 2020; Koga et al., 2005; Li et al., 2017). Recently, it has been discovered that cancer cell-derived EVs may serve as a comprehensive marker to delineate the molecular nature of cancers (Azmi et al., 2013; Ciravolo et al., 2012; Duijvesz et al., 2011; Kahlert and Kalluri, 2013; Li et al., 2017; Munson and Shukla, 2015; Soung et al., 2017; Yamashita et al., 2013; Zhang et al., 2017). To better understand the diagnostic significance and biological functions of cancer-related EVs, it is important to thoroughly characterize EVs produced by established human cancer cell lines on a molecular level (Kahlert and Kalluri, 2013). However, due to the low production and secretion rates, EV yields from cultured human cells is typically on the scale of 10 μg/mL from near confluent to confluent cultures. Consequently, quantification and molecular analysis of EVs in dilute samples such as cell culture media has been challenging.

Despite rapidly growing needs in EV-related researches and diagnostics, there is still no "gold standard" technology available for EV quantification and EV protein analysis. One of the most commonly used approaches in EV detection is based on nanoparticle tracking analysis (NTA) (Franquesa et al., 2014; King et al., 2012; Oosthuyzen et al., 2013). While NTA can non-specifically quantify nano-particles in liquid, it is unable to retrieve any specific molecular information from EVs. On the other hand, traditional biomolecular analysis technologies, such as the Western blotting and mass spectrometry are widely used for

* Corresponding author.
** Corresponding author. Department of Urology, University of Michigan, Ann Arbor, MI, 48109, USA.
E-mail addresses: mday@med.umich.edu (M.L. Day), xsfan@umich.edu (X. Fan).

https://doi.org/10.1016/j.biosx.2021.100066
Received 16 January 2021; Received in revised form 8 May 2021; Accepted 12 May 2021
Available online 20 May 2021

analyzing the protein contents of EVs(Synowsky et al., 2009; Yang et al., 2017). But due to the stringent requirements for the input protein quantity (>5 μg/lane for Western blot and >10 μg/test for mass spectrometry) (Liu, H. et al., 2019b; Sun et al., 2018; Yang et al., 2017), Both of them cannot be used to directly analyze dilute samples such as cell culturing media (Franquesa et al., 2014; Sun et al., 2018). Additionally, EV isolation and purification must be performed in advance using complicated procedures (Greening et al., 2015; Helwa et al., 2017; Lane et al., 2015). Moreover, EV membrane lysis, which is required before protein electrophoresis, makes these two assay impossible to distinguish membrane and cytoplasmic proteins.

Recently, ELISA-based immunoassays have also been used for EV quantification (Franquesa et al., 2014; Tung et al., 2020). As a test that specifically detects the membrane markers (typically based on CD9, CD63, or CD81) on native EVs, ELISA is more suitable for quantifying EVs in unpurified liquid samples (e.g., serum and cell culturing media) (Di et al., 2020). However, conventional plate-based EV ELISA has several well-known problems such as limited sensitivity, large sample consumptions, and long assay time (Tan et al., 2017). Due to the limitations in sensitivity, it is also hard to perform functional membrane protein analysis with plate-based EV ELISA.

Here we present a highly sensitive and multifunctional EV analysis technology that evolved from an automated microfluidic chemiluminescent ELISA platform developed by our group. Benefitted from the employment of the high surface-to-volume ratio (5 mm^{-1}) microfluidic reactors, the averaged diffusion distance of the biomolecules was significantly reduced, thus the efficiencies of the solid-phase immunosorbent reactions were greatly enhanced (Tan et al., 2017, 2018). Thus, for an immunoassay, the limit of detection is improved, the incubation time shortened, and the required amount of a sample is reduced. In this proof-of-concept study, we employed four human bladder cancer cell lines (all of them were derived from bladder cancer patients) as the model systems to evaluate our assay's performance in every-day EV analysis applications. The EVs collected from an immortalized human bladder epithelial cell line, a human foreskin fibroblast cell line, two human breast cancer cell lines and two mouse cell lines were also tested for internal comparison. With a CD9-based EV detection protocol, we were able to achieve rapid EV quantification (<1 h) with a small sample volume (~8 μL), high sensitivity (limit of detection = 8.7×10^7 EV/mL), and high species specificity. To further improve quantification accuracy, we established individualized calibration curves for each cell line (rather than using a general calibration curve) and evaluated the expression levels of CD9 across all of the cell lines. Based on these individualized calibration curves, we performed EV secretion assays with four representative human bladder cancer cell lines at multiple culturing time points.

In addition to EV quantification, we quantified the expression level for a panel of four cancer-related EV membrane proteins (EGFR, HER2, MHC-I, and EpCAM) using an immunoprofiling assay that combines immunoprecipitation and sandwich ELISA. The EV sample does not need to be pre-purified and the assay requires a very small amount of total input protein (40 ng/marker). According to our observation, the expression level of functional EV membrane proteins is stable under external stimulation and is not directly proportional to their expressions on the cellular level, which indicates that the expression profile of the functional proteins on the EV membrane may be able to serve as a robust and unique "molecular fingerprint" for cancer cell lines.

Results

CD9-based EV ELISA

EV-specific membrane markers such as CD9, CD63, and CD81 are widely used to isolate and detect EVs. As a complex particle, an EV naturally contains many identical membrane protein molecules that can serve as the recognition epitopes, which allows us to use a single type of antibody, rather than a pair of different antibodies, as both capture and detection antibody (note that for signal transduction purposes, when the antibody is used as the detection antibody, it is biotinylated). In this study, we chose human CD9 as the target molecule for EV capture, detection, and quantification. The principle of this EV-specific sandwich ELISA is illustrated in Fig. 1. The selected antibody (clone: MEM-61) was designed to specifically bind with the extracellular domain of the human CD9 (Amrollahi et al., 2019; Kischel et al., 2012), and thus has no cross reactivity with EVs derived from other species. In order to maximize EV immobilization efficiency, an excessive amount of capture antibody was immobilized on the reactor's surface (15 μg/mL), through physical adsorption. In addition, noise reduction approaches (such as double-blocking) was used to generate measurement results with low background noises (Tan et al., 2020a). To further enhance assay sensitivity, we used streptavidin poly-HRP to amplify the chemiluminescent signal (Tan et al., 2020a, 2020b).

The first set of experiments were designed to evaluate the quantification performance and specificity of our EV ELISA. Since the expression of CD9 in different cell lines varies significantly across different types of human cell lines, we established individual calibration curves for each cell line. As illustrated in Fig. 2(A), CD9-based EV calibrations were performed with the EVs extracted from 10 cell lines. Four human bladder cancer cell lines were selected as our model system. The EVs collected from an immortalized human bladder epithelial cell line, a human foreskin fibroblast cell line, and two human breast cancer cell lines were also tested for comparison. A mouse bladder cancer cell line and a mouse fibroblast cell line were used as the negative controls. All cell lines were cultured with exosome-depleted FBS. To ensure a fair comparison, the EVs were first isolated from the culturing medium (with ExoQuick-plus isolation kit) after 2–4 days of culturing. Then, we diluted the stock solutions of all isolated EV samples to a uniform protein concentration of 15 μg/mL. The total protein concentrations were quantified via Bradford assay.

The size distributions, high-resolution confocal images, and Western blot results for the purified EVs can be found in Figs. S1, S2, and S3, respectively. Based on the results generated with these conventional analysis technologies, the purified EV samples possessed diameters ranging from 50 to 250 nm, suggesting a stable morphology over the course of analysis. The purities of our EV samples were also high with no cellular contamination observed (see Fig. S3 for EV purity evaluation with Western blot).

The individual calibration curves generated with our EV ELISA can be found in Fig. 2(B) and (C). The chemiluminescent intensities were measured at six different EV concentrations prepared with 3 × serial dilutions (15, 5, 1.67, 0.55, 0.18, and 0 μg/mL of total EV protein, respectively). No signal was observed with the blank controls for all measurements, therefore, there is no need to conduct background subtraction. The calibration curves for the bladder cancer cell lines were close to each other. However, the calibration curves for the remaining four human cell lines differ significantly from each other, confirming the need to generate an individual calibration curve for each cell line. The lower limits of detection (LLODs) for most human cell lines are below or equal to 0.18 μg/mL (1.4 ng/capillary). However, due to low CD9 expression, the LLOD for human foreskin fibroblast was 1.66 μg/mL. No signal was observed with mouse cell line-derived EVs (marked as 0.1 in Fig. 3(B)), indicative of excellent species specificity of our EV ELISA.

As shown in Fig. 2(C), we also explored the LLOD for EVs that contains the highest amount of CD9, which were derived from the UM-UC-9 cell line. The LLOD was 9.8 ng/mL (0.08 ng/capillary). Based on NS300 (NTA) measurements, this concentration equals to 8.7×10^7 particles/mL (7×10^5EV per capillary), showing that our EV ELISA is 300 times more sensitive than conventional plate-based ELISA that targets CD9 on the EV membrane). More significantly, benefitted from the high surface-to-volume ratio of the microfluidic reactor, we were able to complete the entire assay within 1 h, including 30 min for EV immobilization, 15 min

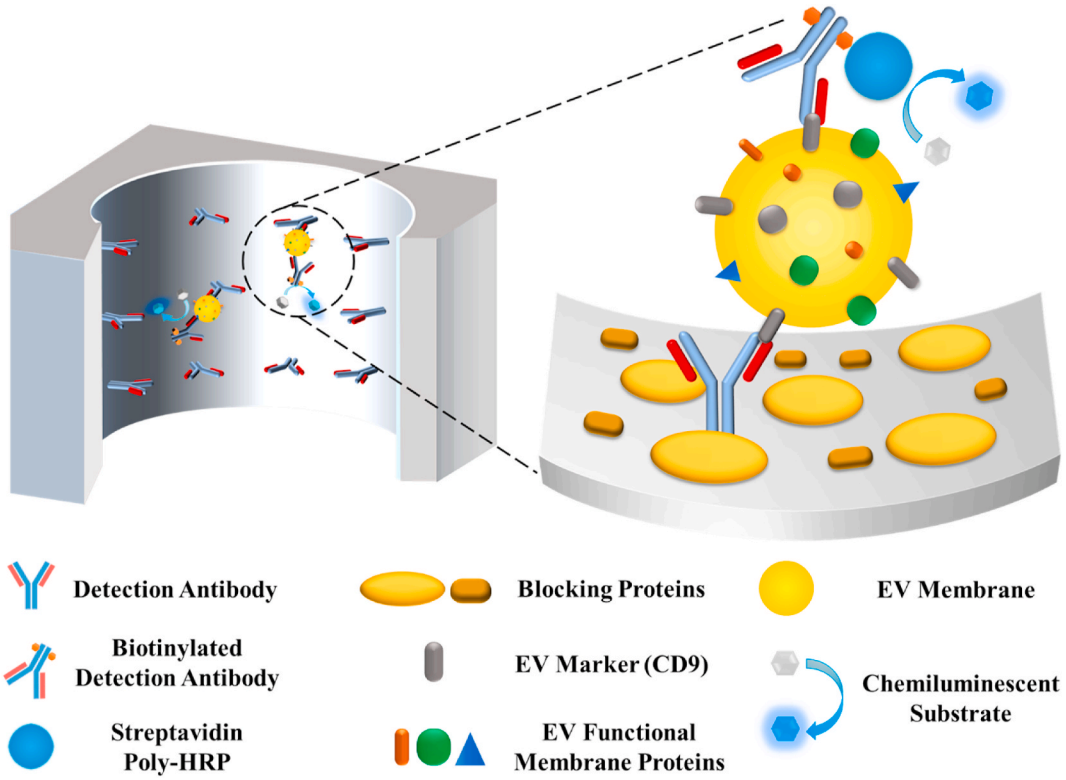

Fig. 1. Illustration of extracellular vesicle (EV) ELISA in a microfluidic ELISA reactor. The assay follows a sandwich immunoassay protocol. For the EV quantification assay, the capture and detection antibodies were selected to bind with the EV's membrane markers (CD9 in our assay).

for detection antibody incubation, 5 min for streptavidin poly-HRP incubation, and 5 min for rinsing, much shorter than conventional plate-based ELISA that requires at least 5 h. With the multiple-exposure approach for chemiluminescent intensity measurements (as shown in Fig. 2(D)), our EV ELISA's linear dynamic ranges are typically larger than three orders of magnitude (the dynamic range of conventional EV ELISA can only cover 2-orders of magnitudes) (Di et al., 2020; SBI; Tan et al., 2020b).

To better visualize the differences in EV-CD9 expressions across the 8 human cell lines, Fig. 2(E) plots, in the descending order, the chemiluminescent intensities at 5 μg/mL (40 ng/mL per capillary) of input protein concentration that are well within the dynamic ranges of the calibration curves for all cell lines. The CD9 expression levels on EVs for the first 7 cell lines are within one order of magnitude and they are 1–2 orders of magnitude higher than the CD9 expression in human foreskin fibroblast-derived EVs. To ensure a similar EV capture efficiency, the human foreskin fibroblast will be excluded in the following experiments.

EV secretion assay for the four bladder cancer cell lines

To examine the practicability in every day EV quantification applications, we conducted an EV secretion assay with the four bladder cancer cell lines, as illustrated in Fig. 3(A). For each cell line, two million cells were first plated on a 15-cm cell culturing plate containing 15 mL of EV-free culturing medium. Then, 0.5 mL of sample was collected at 3 h, 6 h, and 24 h. The entire culturing medium was harvested at the 48th hour. The EV concentrations in the culturing medium at all four time points were then quantified with our CD9-based EV ELISA along with the corresponding calibration curves.

As presented in Fig. 3(B) we were able to detect and quantify EVs even at the earliest sampling time point (3 h). The EV concentrations for all four cell lines have obvious increasing trends during the 48-h surveillance period. From the data at 3 h and 6 h (before the cells started to proliferate), the EV secretion rate for UM-UC-5 is significantly higher than all other three cell lines, whereas UM-UC-3 has the lowest EV secretion rate. These observations suggest that the four similar bladder cancer cell lines have significant variations in EV production and secretion efficiencies.

The immunoprofiling of functional EV membrane proteins

To extract the molecular information about functional proteins on the EV membrane, we developed a quantitative immunoprofiling technology based on the EV ELISA described in the previous sections. The concept and the corresponding procedures of this assay are described in Fig. 4(A) and (B), which are similar to the co-immunoprecipitation assay. A CD9-targeting capture antibody was first used for pulling down EVs from liquid samples. The corresponding antibodies of functional membrane proteins were then added and served as the detection antibodies. The expression of the functional membrane proteins can then be analyzed by measuring the chemiluminescent intensity. Note that each membrane marker under test was measured in separate microfluidic ELISA reactor.

In this proof of concept study, we chose four membrane proteins, EGFR, HER2, MHC1, and EpCAM, which potentially have high diagnostic and therapeutic values for epithelial cell-derived cancers, including bladder cancer. The abnormal expression of these proteins was observed in several famous and widely used epithelial carcinoma cell lines (e.g., the overexpression of EGFR was observed on bladder cancer cell line UM-UC-5; the underexpression of HER2 was observed on breast cancer cell line MDA-MB-231) (Lee-Huang et al., 2000; Osta et al., 2004; Subik et al., 2010; Tamura et al., 2018; Tan et al., 2020a).

We designed a side-by-side study to validate our technology (see Fig. 4(A)) using purified EV samples (with 5 μg/mL of total EV protein) and unpurified cell culturing medium (after 30 min of 10000 g centrifugation to remove cell debris). The concentration of EVs in both groups of samples were first quantified via CD9-based EV ELISA. The chemiluminescent intensities for the functional proteins were then recorded at

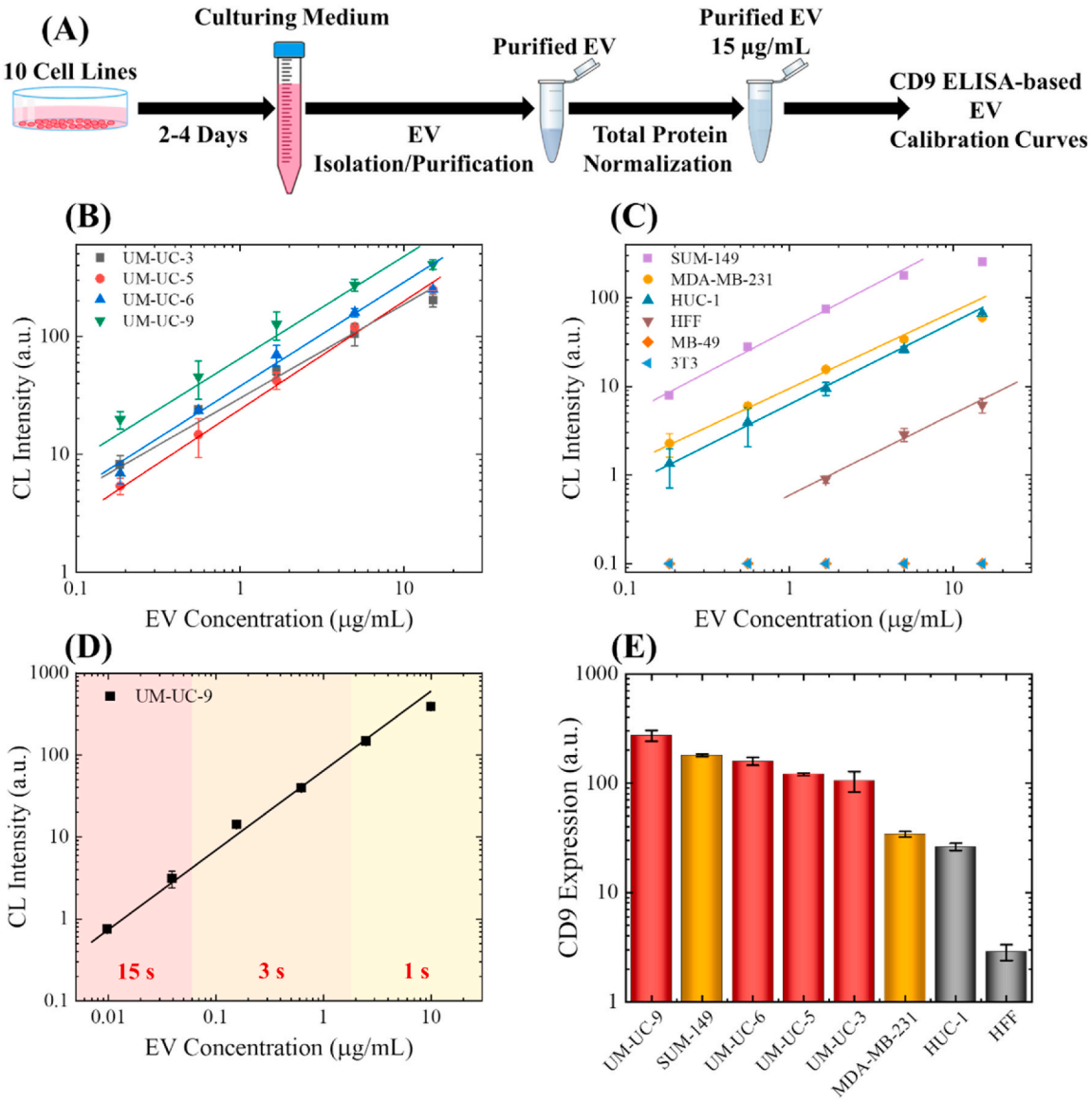

Fig. 2. Cell line specific EV calibration curves. (A) Process to generate EV calibration curves. (B) EV calibration curves generated with bladder cancer cell derived EVs. (C) EV calibration curves generated with breast cancer cell (SUM-149 and MDA-MB-231), bladder epithelial cell (HUC-1), human foreskin fibroblast (HFF), mouse bladder cancer (MB-49), and mouse fibroblast (3T3) derived EV. (D) Entire dynamic range of UM-UC-9 derived EV. The calibration curve was assembled with measurements obtained from multiple camera exposure times. The solid line represents the linear fit in the log-log scale. (E) CD9 expression levels on human cell line derived EVs. The data from the bladder cancer cell lines were labeled with red, the data from breast cancer cell lines were labeled with yellow, and the data from non-cancer cell lines were labeled with grey. All error bars are generated from triplicate measurements. (For interpretation of the references to colour in this figure legend, the reader is referred to the Web version of this article.)

a fixed exposure time (6 s). The background level for each individual marker was also recorded and subtracted from the measurement results. All measurement results lower than the background were marked as 0. For both groups, the signal intensities from all functional proteins were subsequently converted into the "unit signal intensities", which is defined as the signal intensities divided by the calculated EV concentration based on the EV ELISA results.

As shown in the heatmaps in Fig. 4(C) and (D), the expression levels of the functional proteins vary significantly across the seven cell lines. For example, UM-UC-5 and UM-UC-6 have high EGFR expression, whereas UM-UC-3 has a very low level of EGFR. Some of the cell lines do not even express certain markers (e.g., HER2 was not observed on MDA-MB-231-derived EVs). Same as previous studies indicated, the expression level of EV membrane proteinfs does not necessarily correlate with their expression patterns on the cellular level (Welton et al., 2010). For example, the whole cell lysate of UM-UC-6 contains only a moderate amount of EGFR (see Fig. S4), but it expresses a very high level of EGFR on the membrane of EVs. Interestingly, we found that the expression patterns of EV membrane proteins may also be different from their expression patterns in the cellular secretomes. For example, UM-UC-3 and UM-UC-9 secret a large amount of EGFR into the culturing medium (around 1000 pg/mL after 2 days of culturing), but they only express a very low quantity of EGFR on the EV membrane (See Fig. S5). These observations suggest that the expression profile of the functional proteins on the EV may provide unique information about the cells.

For both the purified-EV group and the culturing medium group, high similarities were observed from the triplicate results within each group. To better visualize the EV's similarities and differences within and between the 7 cell lines, we performed a PCA analysis for both groups. As shown in Fig. 4(E) and (F), the data points from the same cell line generally clustered together and the 7 cell lines can easily differentiate from each other. Although the results generated with purified

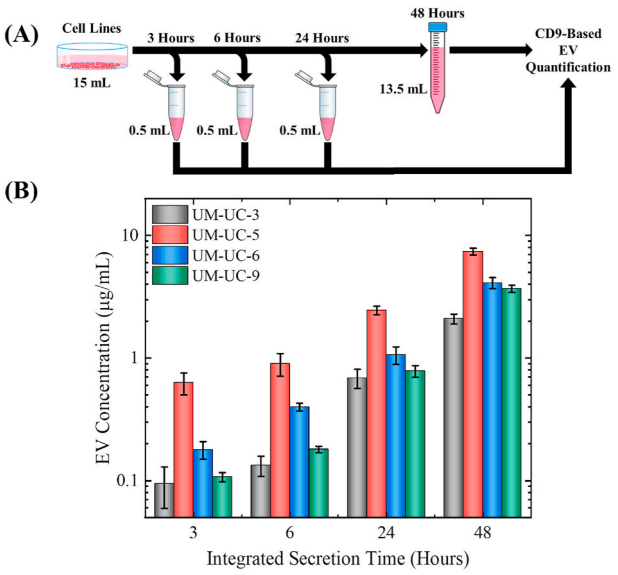

Fig. 3. EV secretion assay with four bladder cancer cell lines. (A) Illustration of the experimental procedure. (B) EV concentration in the culturing medium at four different time points. The error bars are generated from triplicate measurements. UM-UC-5 appears to have the highest EV secretion rate among the four cell lines. All error bars are generated from triplicate measurements.

EVs have slightly better consistency, since the points in the PCA appears to be clustered more closely, the results from both groups do have high similarity in the distribution of the points. The results also indicate that the culturing medium can directly serve as a source of sample for performing EV membrane protein immunoprofiling.

Inhibitors of the EGFR family are widely used in the therapy of epithelial cell-derived cancers through inhibiting the proliferation of the EGFR-expressing cells. To explore the EV responses against such survival stresses, we applied a low concentration of pan-EGFR inhibitor (2 μM of Dacomitinib) to the culturing medium of the seven cell lines. As shown in Fig. 4(C) and (D), EVs derived from UM-UC-5, UM-UC-6, and SUM-149 express the highest amount of EGFR and HER2 (another member in the EGFR family) across these seven cell lines. Due to the high similarities, the EVs from these three cell lines also clustered together on the PCA diagrams (highlighted by the blue regions in Fig. 4(E) and (F). Interestingly, as shown in Fig. S6, these three cell lines within the blue region were also highly sensitive to the pan-EGFR inhibitor—Dacomitinib. Note that the Dacomitinib sensitivity data shown in Fig. S6 agrees with the previously published IC-50 data (Tamura et al., 2018). The examples and explanation of the Dacomitinib inhibition tests can be found in Fig. S7, suggesting that the expression of the EGFR and HER2 on the EV membrane may be indicative of tumor cells' sensitivities to EGFR inhibitors.

Molecular characteristics of EVs after the dacomitinib treatment

With the same survival stress (2 μM of Dacomitinib), we also explored the expression stability of the EV membrane marker protein CD9 with the four bladder cancer cell lines. Same as before, we generated individualized EV calibration curves for all four cell lines with and without the Dacomitinib treatment. As shown in the calibration curves in Fig. S8, decreases in the expression of EV-CD9 were observed in all four bladder cancer cell lines after the Dacomitinib treatment.

A comparison for the expression of EV-CD9 with and without the Dacomitinib treatment can be found in Fig. 5(A). The p-values for the intra-group differences were 0.23, 0.002, 0.02, and 0.01 for UM-UC-3, UM-UC-5, UM-UC-6, and UM-UC-9, respectively. Statistically significance drops ($p < 0.05$) in CD9 expression can be found in the EVs derived from UM-UC-5, UM-UC-6, and UM-UC-9 after the Dacomitinib treatment.

With the new calibration curves, we also quantified the endpoint EV concentrations (in the culturing medium) for the four bladder cancer cell lines with and without the 2 μM Dacomitinib treatment. All samples were collected after 48-h culturing. As shown in Fig. 5(B), although the growth of the tumor cells was obviously inhibited (between 33 and

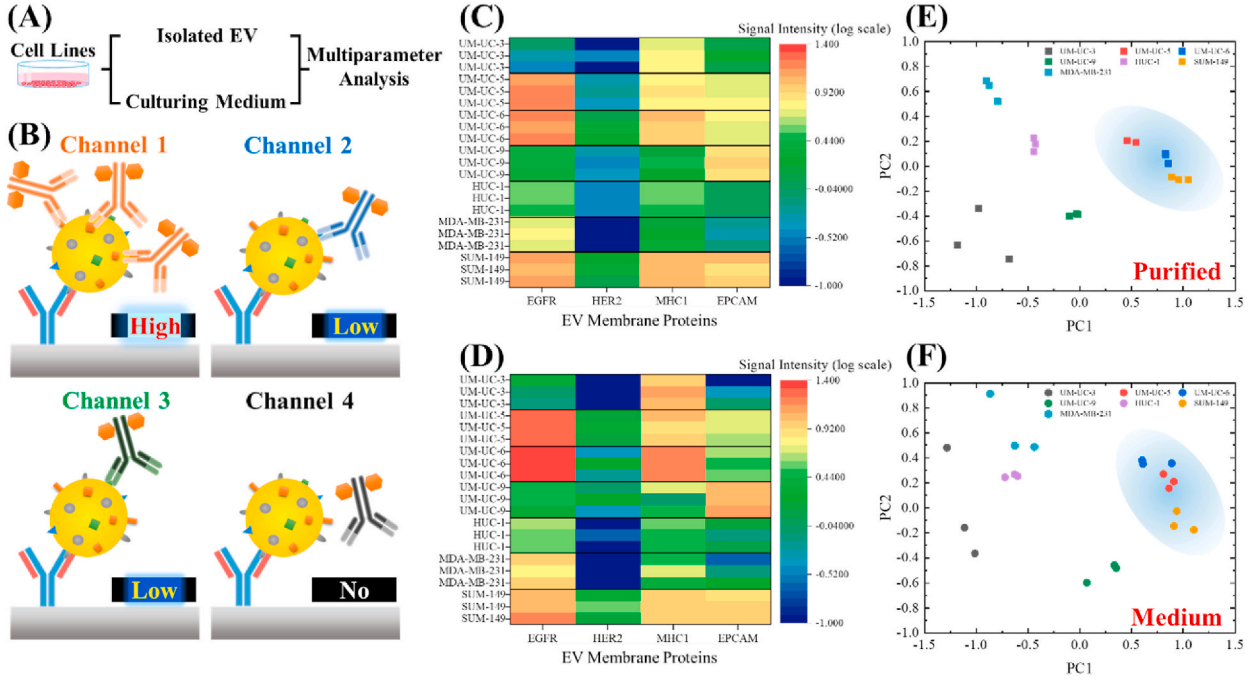

Fig. 4. Functional membrane maker analysis. (A) Procedures for the side-by-side study. (B) Concept illustration for the multi-parameter analysis. A common CD9 capture antibody was used for EV immobilization. Different detection antibodies were used for analyzing the level of various protein expressions. (C)–(D) Heatmaps for the expression of the four selected membrane markers (EGFR, HER2, MHC1, and EpCAM) with purified EV samples (C) and unpurified EVs in cell culturing medium (D). (E)–(F) 4-parameters PCA plots with the purified EV samples (E) and unpurified EVs in cell-culturing medium (F).

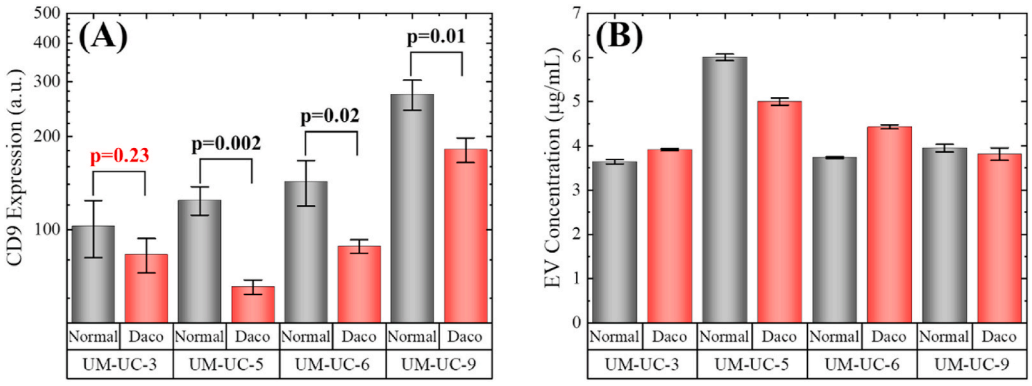

Fig. 5. Secretion response of bladder cancer cell derived EVs after Dacomitinib treatment. (A) Comparison of CD9 expression on the EV with and without Dacomitinib treatment. A significant decrease in CD9 expression was observed from the EVs secreted by UM-UC-5 and UM-UC-6. (B) Endpoint (48 h) EV concentrations calculated based on the new calibration curves. The error bars are generated from triplicate measurements.

74%), the final concentrations of EVs were generally similar between the dacomitinib treatment groups and the normal control groups for three of the four cell lines (except UM-UC-5), suggesting that Dacomitinib treatment may stimulate the production and secretion of EVs for those bladder cancer cell lines. For UM-UC-5, although the cell proliferation was inhibited by 74%, only 17% decrease in the endpoint EV concentration was observed, which is also indicative of increased production and secretion of EVs in response to Dacomitinib treatment.

We also examined the EV expression profiles of the four functional membrane proteins with and without Dacomitinib treatment. Same as we introduced in the previous experiment, the measurements were performed with purified EV and debris-removed cell culturing medium. The EV concentrations in the Dacomitinib-treated groups were measured with the new calibration curves and heatmaps generated from this analysis (Fig. 6(A) and (B)) reveals the intra-group averages for that particular marker.

As shown in Fig. 6(A) and (B), for the four bladder cancer cell lines, we still observed very high similarities between the EVs collected from the normal control group and those collected from the Dacomitinib treatment group. The expression levels of the four functional proteins on the EV membrane remains mostly intact after the Dacomitinib treatment. Same as before, high similarities were observed between the purified EVs and the EVs directly pulled down from the culturing medium. These observations can be further verified with the PCA plots (shown in Fig. 6(C) and (D)). The EVs collected from the Dacomitinib treated groups still clustered with the normal control groups. For UM-UC-5 and UM-UC-6 cell lines, the points corresponding to the EVs collected after the 2 μM Dacomitinib treatment are still located in the blue regions. These observations indicate that an intermediate level of stress (such as the 2 μM Dacomitinib treatment) will not drastically change the expression pattern of the EV membrane protein profile. They further suggest that the functional EV membrane proteins' expression profile may serve as a unique and robust "molecular fingerprint" in the immunophenotyping and molecular analysis of tumor cells.

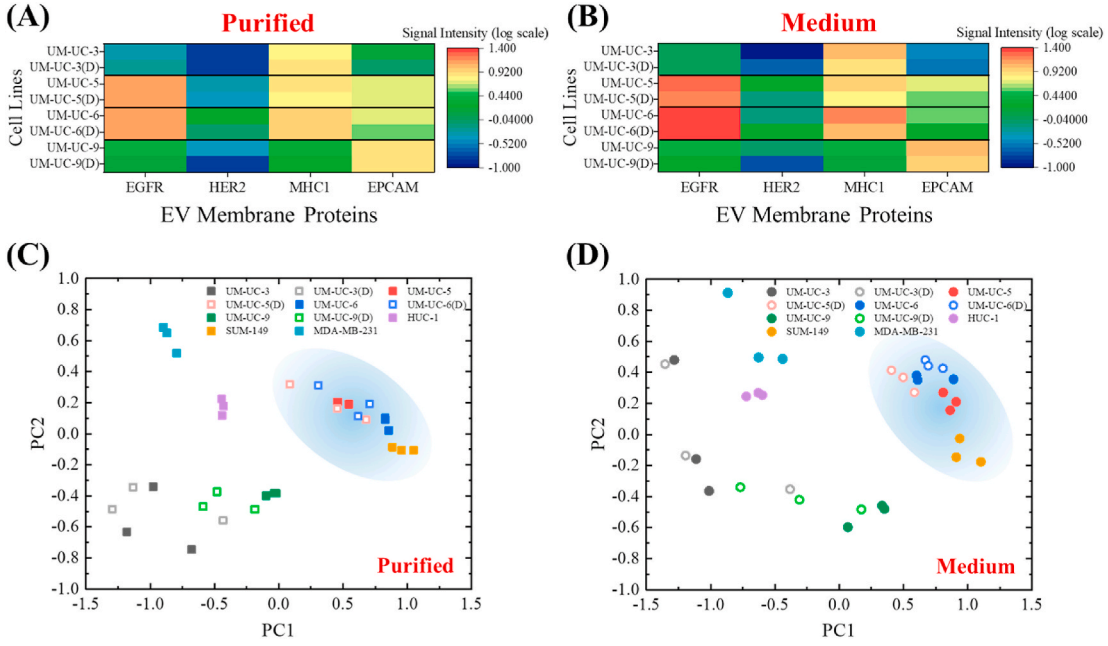

Fig. 6. Expression of the four functional membrane markers after Dacomitinib treatment with the EVs collected from the four bladder cancer cell lines. (A)–(B) Heatmaps for the expression of the four membrane markers (EGFR, HER2, MHC1, and EpCAM) with and without Dacomitinib stimulation with the purified EV samples (A) and unrefined EVs in cell culturing medium (B). (C)–(D) PCA plots with the purified EV samples (C) and unrefined EVs in cell culturing medium (D) with and without Dacomitinib treatment. Note that the label "(D)" in the figure legends denotes the EVs collected from the Dacomitinib treated groups (shown as the hollow squares and hollow circles on the plots).

Discussion and conclusion

In this study, we have successfully demonstrated a microfluidic biosensing platform for EV quantification and molecular analysis. On this platform, EV quantification was achieved through CD9-based chemiluminescent ELISA. Benefitting from the employment of microfluidic ELISA reactors, we were able to complete the entire assay within 1 h and with 8 μL of the input sample volume. With adjustable exposure times, we were able to generate calibration curves with the EVs that were purified from multiple human cell lines. For the cell lines with high EV-CD9 expressions, the LLOD can be as low as 8.7×10^7 EV/mL (7×10^5 EV/capillary), which is around 300 times more sensitive than conventional plate-based EV ELISAs. With the current cell culturing protocol, this EV quantification assay is robust and reproducible (see Fig. S9).

The novel EV molecular analysis technology was developed based on the aforementioned EV ELISA technology. In particular, it is an immunoprofiling technology that can quantitatively evaluate the expression level of functional EV membrane proteins. For the analysis of common epithelial cancer markers such as EGFR, HER2, MHC1, and EpCAM, our immunoprofiling assay only requires a very small amount of total input protein (<5 μg/mL, 40 ng/capillary), which is > 100 times less than the required protein quantity for Western blot (>5 μg/lane). A comparison chart for the performances of EV biomolecular analysis technologies can be found in Table S1. With this high sensitivity, EV isolation is no longer pre-requisite for performing biomolecular assays. Cell culturing medium collected 1–2 days after the cell inoculation can directly serve as the sample for EV membrane protein analysis.

Indeed, many other types of EV isolation, quantification, and analysis technologies have been recently developed based on the concept of microfluidic biosensing, some of which show very good performance in EV-related applications (Im et al., 2014; Kanwar et al., 2014; Liu, C. et al., 2019a; Lo et al., 2020). However, a large portion of them involve sophisticated fluidic designs (Im et al., 2014) and suffer from problems such as strong background noise (due to insufficient rinsing) and questionable reproducibility (due to limitations in signal transduction mechanisms) (Min et al., 2020; Zhang et al., 2016). In contrast, the simple reactor structure, automated reagent handling procedures, and well-optimized assay protocols make our EV ELISA and EV immunoprofiling assays highly reproducible with very low background noise (Tan et al., 2017, 2020a). Our results should also be comparable with the results generated with traditional ELISA, as they share the same signal transduction mechanism.

In addition to the engineering achievements, we had several interesting biological findings. First, EVs' production rate varies significantly, even between bladder cancer cell lines with similar origins. Second, the abundance of functional membrane proteins on the EVs does not strictly correlate with their expression, on either the cellular level or the cell secretome level. Third, EVs derived from completely different cell types (such as the bladder cancer cell lines UM-UC-5, UM-UC-6, and the breast cancer cell line SUM-149) can have high similarities on the molecular level. Forth, while the expression levels of the EV membrane markers (such as CD9) may change under survival stress (such as the 2 μM Dacomitinib), the expression profiles of the functional membrane proteins are relatively robust under the same survival stress. Fifth, the abundance of EV-EGFR as well as other proteins in the EGFR family (such as HER2), may be indicative of tumor cells' sensitivities against EGFR inhibitors. All of these observations indicate that the molecular information contained in the EVs may serve as a unique "fingerprint" in the immunophenotyping and molecular analysis of tumor cells. The mechanisms and the biological significance behind these observations are certainly worth further investigation.

In the future, we will explore the performance of this EV analysis platform under other conditions. In the current study, we only examined the EVs that express CD9 on its membrane. To examine the differences and similarities among different EV subpopulations (Willms et al., 2016), we can employ other types of antibodies (such as the anti-CD63 and anti-CD81 antibodies) for EV immobilization, as long as antibodies with high affinity and high specificity are available. Additionally, instead of using ExoQuick, we will explore other EV purification methods such as density gradient ultracentrifugation and size exclusion chromatography for EV isolation and purification (Benedikter et al., 2017; Brennan et al., 2020; de Menezes-Neto et al., 2015; Koh et al., 2018). Finally, we will integrate our EV ELISA platform with other EV analysis methodologies. As exemplified in Fig. S10, after isolating the desired EV subpopulations (e.g., EGFR + EV), we can further investigate their molecular characteristics using various novel approaches, including proteomic analysis (such as the immunoprofiling technology which was presented in this paper) and nucleic acid analysis (such as RNA sequencing). Besides, the immunoprofiling concept presented in this paper can also be applied to the biomolecular analysis of other nanometer-sized complex particles such as viruses.

The current version of our EV analysis technology still has a few technical limitations, such as the relatively low assay throughput. It can be improved by incorporating a microfluidic-s based immunoassay reactor that has multiplexing capability. Besides, the assay itself also worth further optimization. For example, we observed relatively large intra-group variances in both the quantification section and the immunoprofiling section. It is hypothetically caused by the inter-particle variations of the EVs(Willms et al., 2016) and/or the low affinity between the antibodies and the EV membrane proteins. This problem can be potentially improved by employing antibodies with better affinities and specificities or using EV purification methodologies that can generate cleaner products. It is also worth noting that our assay may not be sensitive enough to analyze the EV abundance of low-expression proteins. For example, we could not detect the bladder cancer marker ADAM15 with 5 μg/mL of input EV protein. To detect this marker on the EV membrane, we had to increase the input quantity of EV protein to 30 μg/mL (see Fig. S11). To resolve this problem, antibodies with higher binding affinities should be used. A low-noise signal amplification approach may also be necessary.

Materials & methods

Cell culturing

The UM-UC-3, UM-UC-5, UM-UC-6, UM-UC-9 and HUC-1 cell lines were obtained from their originator, Dr. H. Barton Grossman of the MD Anderson Cancer Center (Houston, TX). Cells were first cultured in Dulbecco's Modified Eagle Medium (HyClone) supplemented with 8% fetal bovine serum (Thermo Fisher), 1% penicillin-streptomycin-Fungizone (Lonza BioWhittaker), and 2 mM GlutaMAX (Thermo Fisher Gibco). Cells were grown in a humidified incubation chamber at 5% CO2 and 37 °C. Cell line authenticity was verified by analysis of short tandem repeats (IDEXX Bioanalytics) and lines were determined mycoplasma free by PlasmoTest (InvivoGen).

The MDA-MB-231 cell line was obtained from ATCC. Human Foreskin Fibroblasts was a gift from Trojanowska Lab. They were first cultured in high glucose DMEM containing 1% penicillin/streptomycin, L-glutamine, and 8% of FBS.

Once each cell line reached 80% confluency, they were plated into new 150 mm culturing dishes (approximately two million cells) in normal growth medium. When cells reached 60% confluency the normal growth media was discarded and the EV-free culturing media was added to the culture dish. The EV-free culturing media (8% exosome-depleted FBS, (Thermo Fisher Gibco A2720803) in DMEM), no other supplements were added. Note that for Dacomitinib-related experiments, DMSO-dissolved Dacomitinib (Sigma PZ0330) was mixed with the EV-free culturing media at a final concentration of 2 μM. 48 h following the addition of the EV-free culturing media, the media was harvested for analysis. At harvest, the cell supernatants were centrifuged at low speed for 5 min to remove dead cells. The cell pellets (dead cells) were

discarded. Harvested supernatants were aliquoted into new polypropylene conical centrifuge tubes and stored at 4 °C until EV purification.

Cell counting and cell imaging

Following the harvest of cell culturing media, the remaining attached cells were counted. Attached cells (in the 150 mm dishes) were washed with PBS and subjected to trypsinization then single cell suspensions were analyzed for viability and cell number using an automated cell counter (BioRad TC20). Bright field photomicrographs were taken on Olympus inverted microscope CKX41 with Olympus camera system DP72.

EV isolation and purification

The isolation of EV from the cell culturing medium was performed using a protocol that combines differential centrifugation and polymer precipitation-based EV isolation. First, cells or dead cells were removed from the cell culturing medium with 15 min of centrifugation under 1500×*g*. Then, smaller cell debris was removed with 30 min of centrifugation under 10000×*g*. The second half of the EV isolation was performed with the ExoQuick-TC Plus kit (System Bioscience EQPL10TC-1). Briefly, we first mixed the ExoQuick-TC solution with the pre-treated cell culturing mediums (with volumetric ratio at 1:5). Then, we incubated the mixed samples overnight at 4 °C. Then, we centrifuged the cell culturing mediums for 30 min, under 3000×*g*. Finally, the products of the EV isolation assay were further purified using the columns provided in the ExoQuick.

EV characterization

Four different methods were used to characterize the purified EVs. The total protein concentrations in the purified EV samples were quantified using a Bradford assay kit (Thermo Fisher 23236), following the provided procedure. For the ease of subsequent ELISA analysis, we diluted the total protein concentrations of all purified EV samples to 15 μg/mL. We also characterized the size distributions and the purities of the EV samples, using nanoparticle tracking analysis (Nanosight NS300), high-resolution confocal imaging (Zeiss LSM800), and Western blotting. The protocols of these three assays can be found in the supplementary information.

Microfluidic ELISA system

The detailed description of the microfluidic chemiluminescent ELISA system can be found in our previous publications (Tan et al., 2018). 12-channel polystyrene capillaries were used as the ELISA reactors. The inner surface of each capillary is a hollow tube with an 800 μm diameter. A liquid pump (multi-channel pipette) was used to control the flow of the liquid reagents. A CMOS camera was used to quantify the chemiluminescent signal of the ELISA reaction (Tan et al., 2017, 2018). A photo of the microfluidic chemiluminescent ELISA system can be found in Fig. S12.

ELISA reagents

For EV quantification assay, a monoclonal antibody that binds specifically with human CD9 was used (clone number: MEM-61). The unconjugated version of MEM-61 (Thermo Fisher MA1-19002) was used as the capture antibody. The biotinylated version of MEM-61 (Thermo Fisher MA1-19485) was used as the detection antibody. The working solution of the capture antibody was prepared at 15 μg/mL and the working solution of the detection antibody was prepared at 1 μg/mL.

For EV membrane protein immunoprofiling assays, 15 μg/mL of MEM-61 anti-CD9 antibody was still used as the capture antibody. The detection antibodies for EGFR, HER2, EPCAM, and ADAM15 were purchased from R&D systems. The detection antibody for MHC-1 was purchased from Thermo Fisher. Their catalog numbers are BAF231 (EGFR), BAF1129 (HER2), BAF960 (EPCAM), BAF935 (ADAM15) and 13-9983-82 (MHC-1). The working concentrations of the detection antibodies were determined by a series of optimization experiments (aiming for high signal-to-noise ratio at 6 s of exposure time). The working solutions of the detection antibodies were prepared at the following concentrations: 1 μg/mL for EGFR detection antibody, 0.5 μg/mL for HER2 detection antibody, 0.4 μg/mL for EPCAM detection antibody, 0.5 μg/mL for ADAM15 detection antibody, and 1 μg/mL for MHC-1 detection antibody. The working solutions of the capture antibody was prepared with 1x PBS and the working solutions for all detection antibodies were prepared with 1% BSA in 1 × PBS.

As we described in our previous publications, the capture antibody coating buffer (1x PBS, DY006), concentrated wash buffer (WA126), and concentrated reagent diluent (10% BSA in 10 × PBS, DY995) were purchased from R&D Systems. The working solution of the wash buffer and reagent diluent were diluted with Milli-Q water (R = 18.2 Ω) to achieve 1x working concentration (based on user's manual). The Superblock PBS buffer (ThermoFisher, 37518), the streptavidin poly-HRP stock solution (ThermoFisher, 21140) and the poly-HRP dilution buffer (1% casein in 1x PBS, ThermoFisher, N500) were purchased from Thermo Fisher. The working solution for the streptavidin poly-HRP was prepared by diluting the stock solution 1500 times with the poly-HRP dilution buffer. The chemiluminescent substrate (SuperSignal ELISA Femto Substrate, ThermoFisher, 37075) was used for detection. The working substrate solution was prepared by equal-volumetric mixing of the Luminol + Enhancer Solution and the Stable Peroxide Solution (all contained in the substrate kit) at room temperature.

ELISA protocol

A graphical illustration of the common protocol for the CD9-based EV ELISA and the EV membrane protein immunoprofiling assays can be found in Fig. S13. The first 115 min were used for sensor preparation, including 60 min for capture antibody immobilization, 45 min for blocking with 1% BSA, and 10 min for blocking with Superblock buffer. Note that the sensor preparation steps can be done in advance. The actual assay time was about 55 min, including 30 min for EV sample incubation, 15 min for detection antibody incubation and 5 min for streptavidin poly-HRP incubation. Note that a rinsing step (with 0.05% Tween) was performed after each incubation step.

Principal component analysis (PCA)

To reduce dimensionality for classification we applied PCA analysis with the 4-proteins immunoprofiling results. A common logarithm operation was first applied to all chemiluminescent intensity measurements. A set of the measurements results that were generated with the purified EVs (without Dacomitinib treatment) was defined as the training set (containing 21 sets of data). All other groups of data were defined as the testing set. PCA was first applied to the 21-by-4 dataset (training set) to produce 21-by-4 principal component scores. As shown in Fig. S14, approximately 88% of the variability was explained with the first two PCs. Hence, we selected the primary two principal components for to perform data visualization. With the 4-by-4 PCA coefficients acquired from the training set, the PC scores of the testing set can be calculated by multiplying the PCA coefficients to the testing samples' dataset.

CRediT authorship contribution statement

Xiaotian Tan: Conceptualization, Methodology, Investigation, Formal analysis, Writing – original draft. **Kathleen C. Day:** Methodology, Investigation. **Xuzhou Li:** Investigation, Formal analysis. **Luke J.**

Broses: Investigation. **Wen Xue:** Investigation. **Weishu Wu:** Investigation. **William Y. Wang:** Investigation. **Ting-Wen Lo:** Investigation. **Emma Purcell:** Investigation. **Sicong Wang:** Conceptualization, Methodology. **Yun-Lu Sun:** Investigation. **Maung Kyaw Khaing Oo:** Methodology, Investigation, Resources, Formal analysis, Writing – original draft. **Brendon M. Baker:** Resources, Writing – original draft. **Sunitha Nagrath:** Resources, Writing – original draft. **Mark L. Day:** Conceptualization, Methodology, Resources, Writing – original draft. **Xudong Fan:** Conceptualization, Formal analysis, Resources, Supervision, Writing – original draft.

Declaration of competing interest

The authors declare the following competing financial interest): M. K. K. O. and X. F. are co-founders of and have an equity interest in Optofluidic Bioassay, LLC.

Appendix A. Supplementary data

Supplementary data to this article can be found online at https://doi.org/10.1016/j.biosx.2021.100066.

References

Amrollahi, P., Rodrigues, M., Lyon, C.J., Goel, A., Han, H., Hu, T.Y., 2019. Front. Genet. 10, 1273.

Azmi, A.S., Bao, B., Sarkar, F.H., 2013. Canc. Metastasis Rev. 32 (3–4), 623–642.

Benedikter, B.J., Bouwman, F.G., Vajen, T., Heinzmann, A.C., Grauls, G., Mariman, E.C., Wouters, E.F., Savelkoul, P.H., Lopez-Iglesias, C., Koenen, R.R., Rohde, G.G.U, Stassen, F.R.M., 2017. Sci. Rep. 7 (1), 1–13.

Brennan, K., Martin, K., FitzGerald, S.P., O'Sullivan, J., Wu, Y., Blanco, A., Richardson, C., Mc Gee, M.M., 2020. Sci. Rep. 10 (1), 1–13.

Ciravolo, V., Huber, V., Ghedini, G.C., Venturelli, E., Bianchi, F., Campiglio, M., Morelli, D., Villa, A., Mina, P.D., Menard, S., Filipazzi, P., Rivoltini, L., Tagliabue, E., Pupa, S.M., 2012. J. Cell. Physiol. 227 (2), 658–667.

de Menezes-Neto, A., Sáez, M.J.F., Lozano-Ramos, I., Segui-Barber, J., Martin-Jaular, L., Ullate, J.M.E., Fernandez-Becerra, C., Borrás, F.E., Del Portillo, H.A., 2015. J. Extracell. Vesicles 4 (1), 27378.

Di, H., Mi, Z., Sun, Y., Liu, X., Liu, X., Li, A., Jiang, Y., Gao, H., Rong, P., Liu, D., 2020. Theranostics 10 (20), 9303.

Duijvesz, D., Luider, T., Bangma, C.H., Jenster, G., 2011. Eur. Urol. 59 (5), 823–831.

Franquesa, M., Hoogduijn, M.J., Ripoll, E., Luk, F., Salih, M., Betjes, M.G., Torras, J., Baan, C.C., Grinyó, J.M., Merino, A.M., 2014. Front. Immunol. 5, 525.

Gartz, M., Strande, J.L., 2018. J. Am. Heart Assoc. 7 (11), e007954.

Greening, D.W., Xu, R., Ji, H., Tauro, B.J., Simpson, R.J., 2015. Methods Mol. Biol. 179–209.

Helwa, I., Cai, J., Drewry, M.D., Zimmerman, A., Dinkins, M.B., Khaled, M.L., Seremwe, M., Dismuke, W.M., Bieberich, E., Stamer, W.D., Hamrick, M.W., Liu, Y., 2017. PloS One 12 (1), e0170628.

Im, H., Shao, H., Park, Y.I., Peterson, V.M., Castro, C.M., Weissleder, R., Lee, H., 2014. Nat. Biotechnol. 32 (5), 490–495.

Kahlert, C., Kalluri, R., 2013. J. Mol. Med. 91 (4), 431–437.

Kalluri, R., LeBleu, V.S., 2020. Science 367 (6478).

Kanwar, S.S., Dunlay, C.J., Simeone, D.M., Nagrath, S., 2014. Lab Chip 14 (11), 1891–1900.

King, H.W., Michael, M.Z., Gleadle, J.M., 2012. BMC Canc. 12 (1), 1–10.

Kischel, P., Bellahcene, A., Deux, B., Lamour, V., Dobson, R., De Pauw, E., Clezardin, P., Castronovo, V., 2012. Anticancer Res. 32 (12), 5211–5220.

Koga, K., Matsumoto, K., Akiyoshi, T., Kubo, M., Yamanaka, N., Tasaki, A., Nakashima, H., Nakamura, M., Kuroki, S., Tanaka, M., Katano, M., 2005. Anticancer Res. 25 (6A), 3703–3707.

Koh, Y.Q., Almughlliq, F.B., Vaswani, K., Peiris, H.N., Mitchell, M.D., 2018. Front. Biosci. 23, 865–874.

Kowal, J., Arras, G., Colombo, M., Jouve, M., Morath, J.P., Primdal-Bengtson, B., Dingli, F., Loew, D., Tkach, M., Théry, C., 2016. Proc. Natl. Acad. Sci. U.S.A. 113 (8), E968–E977.

Lane, R.E., Korbie, D., Anderson, W., Vaidyanathan, R., Trau, M., 2015. Sci. Rep. 5, 7639.

Lee-Huang, S., Huang, P.L., Sun, Y., Chen, H.C., Kung, H.F., Murphy, W.J., 2000. Anticancer Res. 20 (2A), 653–659.

Li, W., Li, C., Zhou, T., Liu, X., Liu, X., Li, X., Chen, D., 2017. Mol. Canc. 16 (1), 145.

Liu, C., Zhao, J., Tian, F., Cai, L., Zhang, W., Feng, Q., Chang, J., Wan, F., Yang, Y., Dai, B., Cong, Y., Ding, B., Sun, J., Tan, W., 2019a. Nat. Biomed. Eng. 3 (3), 183–193.

Liu, H., Sun, X., Gong, X., Wang, G., 2019b. J. Cell. Biochem. 120 (9), 14455–14464.

Lo, T.-W., Zhu, Z., Purcell, E., Watza, D., Wang, J., Kang, Y.-T., Jolly, S., Nagrath, D., Nagrath, S., 2020. Lab Chip 20 (10), 1762–1770.

Min, J., Son, T., Hong, J.S., Cheah, P.S., Wegemann, A., Murlidharan, K., Weissleder, R., Lee, H., Im, H., 2020. Adv. Biosyst. 2000003.

Munson, P., Shukla, A., 2015. Medicine 2 (4), 310–327.

Oosthuyzen, W., Sime, N.E., Ivy, J.R., Turtle, E.J., Street, J.M., Pound, J., Bath, L.E., Webb, D.J., Gregory, C.D., Bailey, M.A., Dear, J.W., 2013. J. Physiol. 591 (23), 5833–5842.

Osta, W.A., Chen, Y., Mikhitarian, K., Mitas, M., Salem, M., Hannun, Y.A., Cole, D.J., Gillanders, W.E., 2004. Canc. Res. 64 (16), 5818–5824.

SBI, https://systembio.com/shop/exosome-elisa-complete-kit-cd9-detection/. 10/23/2020).

Soung, Y.H., Ford, S., Zhang, V., Chung, J., 2017. Cancers 9 (1), 8.

Subik, K., Lee, J.-F., Baxter, L., Strzepek, T., Costello, D., Crowley, P., Xing, L., Hung, M.-C., Bonfiglio, T., Hicks, D.G., Tang, P., 2010. Breast Cancer 4, 117822341000400004.

Sun, Y., Huo, C., Qiao, Z., Shang, Z., Uzzaman, A., Liu, S., Jiang, X., Fan, L.Y., Ji, L., Guan, X., Cao, C.X., Xiao, H., 2018. J. Proteome Res. 17 (3), 1101–1107.

Synowsky, S.A., van Wijk, M., Raijmakers, R., Heck, A.J., 2009. J. Mol. Biol. 385 (4), 1300–1313.

Tamura, S., Wang, Y., Veeneman, B., Hovelson, D., Bankhead III, A., Broses, L.J., Lorenzatti Hiles, G., Liebert, M., Rubin, J.R., Day, K.C., Hussain, M., Neamati, N., Tomlins, S., Palmbos, P.L., Grivas, P., Day, M.L., 2018. Bladder Cancer 4 (1), 77–90.

Tan, X., Broses, L.J., Zhou, M., Day, K.C., Liu, W., Li, Z., Weizer, A.Z., Munson, K.A., Khiang Oo, M.K., Day, M.L., 2020. Lab Chip 20 (3), 634–646.

Tan, X., David, A., Day, J., Tang, H., Dixon, E.R., Zhu, H., Chen, Y.-C., Khaing Oo, M.K., Shikanov, A., Fan, X., 2018. ACS Sens. 3 (11), 2327–2334.

Tan, X., Krel, M., Dolgov, E., Park, S., Li, X., Wu, W., Sun, Y.-L., Zhang, J., Khiang Oo, M. K., Perlin, D.S., Fan, X., 2020b. Biosens. Bioelectron. 112572.

Tan, X., Khiang Oo, M.K., Gong, Y., Li, Y., Zhu, H., Fan, X., 2017. Analyst 142 (13), 2378–2385.

Tung, S.L., Fanelli, G., Matthews, R.I., Bazoer, J., Letizia, M., Vizcay-Barrena, G., Faruqu, F.N., Philippeos, C., Hannen, R., Al-Jamal, K.T., Lombardi, G., Smyth, L.A., 2020. Front. Cell Dev. Biol. 8, 317.

Welton, J.L., Khanna, S., Giles, P.J., Brennan, P., Brewis, I.A., Staffurth, J., Mason, M.D., Clayton, A., 2010. Mol. Cell. Proteomics 9 (6), 1324–1338.

Willms, E., Johansson, H.J., Mäger, I., Lee, Y., Blomberg, K.E.M., Sadik, M., Alaarg, A., Smith, C.E., Lehtiö, J., Andaloussi, S.E., Wood, M.J.A., Vader, P., 2016. Sci. Rep. 6 (1), 1–12.

Yamashita, T., Kamada, H., Kanasaki, S., Maeda, Y., Nagano, K., Abe, Y., Inoue, M., Yoshioka, Y., Tsutsumi, Y., Katayama, S., Inoue, M., Tsunoda, S., 2013. Pharmazie 68 (12), 969–973.

Yang, C., Guo, W.B., Zhang, W.S., Bian, J., Yang, J.K., Zhou, Q.Z., Chen, M.K., Peng, W., Qi, T., Wang, C.Y., Liu, C.D., 2017. Andrology 5 (5), 1007–1015.

Zhang, H., Deng, T., Liu, R., Bai, M., Zhou, L., Wang, X., Li, S., Wang, X., Yang, H., Li, J., Zhang, L., Ying, G., Ba, Y., 2017. Nat. Commun. 8 (1), 1–11.

Zhang, P., He, M., Zeng, Y., 2016. Lab Chip 16 (16), 3033–3042.